

## Cooling rate dependent morphology of the $\gamma'$ precipitates in nickel-base superalloy *Udimet 500*

Mohammad Khalili Savadkoohi<sup>a</sup>, Ahad Samadi<sup>b</sup>, Rasoul Salehi<sup>c</sup>

Faculty of Materials Engineering, Sahand University of Technology, Tabriz, P.O. Box: 51335-1996, Iran.

Tel./Fax: +98 412 3459434/+98 412 3444333.

<sup>a</sup>m.kh.savadkoohi@gmail.com, <sup>b</sup>samadi@sut.ac.ir, <sup>c</sup>r\_salehi@sut.ac.ir

**Key words:** Morphology, electrolytic extraction, constrained, unconstrained, elastic strain,  $\gamma'$  precipitation.

**Abstract.** The morphology of the  $\gamma'$  precipitates during continues cooling of a nickel-base superalloy, *Udimet 500*, was studied using scanning electron microscopy and X-ray diffraction technique. The samples were full solutioned at 1200°C and then were cooled to ambient temperature under different cooling rates, 15, 1, 0.2, 0.05°C/min and air cooling. The unconstrained  $\gamma$ - $\gamma'$  misfit values for each sample were calculated using the electrolytic extracted  $\gamma'$  precipitates. According to the results, by decreasing the cooling rate, not only the size, volume fraction and interparticle spaces of the  $\gamma'$  precipitates were increased, but also depending on the  $\gamma$ - $\gamma'$  lattice misfits the corresponding  $\gamma'$  morphology was changed from spherical to cubic, then flower-like and finally dendritic shape. The observations are discussed in view of the compositional changes of  $\gamma/\gamma'$  phases and elastic strain considerations of their interfaces which will be described in detail in the article.

### 1. Introduction

It is well known that the precipitation of coherent  $\gamma'$  phase in the matrix phase  $\gamma$  is responsible for the stable strength of the nickel-base superalloys at high temperature applications. Depending on thermal history and treatments, a variety of morphologies has been observed in the alloy microstructure for the  $\gamma'$  precipitates which can affect on the mechanical and microstructural stability during high temperature services [1, 2].

The morphology of the  $\gamma'$  particles depends on not only the elastic strain energy associated with the  $\gamma$ - $\gamma'$  lattice misfit, but also the interparticle spaces attributing to nucleation rate, volume fraction and sizes of the precipitates. The number density, volume fractions and sizes of the precipitates through influencing on the interparticle spaces hence interaction of the elastic strain fields of near precipitates, change the particles morphology and their thermal stability. So in solution treatment the cooling rate through affecting on above mentioned microstructural characteristics can play an effective role in morphological evolutions [1-6].

The lattice misfit between  $\gamma'$  and  $\gamma$ , is given by Eq. 1.

$$\delta = \frac{2(a_{\gamma'}^p - a_{\gamma})}{a_{\gamma'}^p + a_{\gamma}} \quad (1)$$

where  $\delta$  and  $a_{\gamma'}^p$  are the unconstrained lattice misfit and lattice constant of the extracted  $\gamma'$  precipitates from the bulk sample, respectively, and  $a_{\gamma}$  is the lattice constant of the matrix phase [7]. In addition, the difference between the lattice constant for the constrained,  $a_{\gamma'}^b$ , and unconstrained  $\gamma'$  leads to an elastic strain,  $\varepsilon_e$ , in constrained  $\gamma'$  which is calculated by Eq. 2, [8].

$$\varepsilon_e = \frac{a_{\gamma'}^b - a_{\gamma'}^p}{a_{\gamma'}^p}. \quad (2)$$

In fact, the elastic strain is a direct result of the slight difference between the  $\gamma$  and  $\gamma'$  lattice constants which is attributed to their coherency condition.

In this research, through a systematic investigation, the morphological evolution of the  $\gamma'$  precipitates has been studied in a commercial nickel-base superalloy, *Udimet 500*, during continues cooling from the full solutioned state. These morphological variations have been analyzed through elastic strain aspects in  $\gamma/\gamma'$  interfaces.

## 2. Experimental procedures

The investment cast carrot shape samples of a nickel-base superalloy, *Udimet 500*, with a chemical composition: 19.1 Cr, 16.2 Co, 3.7 Al, 3.05 Ti, 4.2 Mo, 0.4 Fe, 0.02 C, 0.02 Si and balance nickel in weight percent were used for sampling. Then disk shape samples with a 3mm height and 10 mm diameter were cut from the carrots for heat treatment. The samples were full solutioned to obtain an identical morphology [1, 2] to attribute a unique  $\gamma/\gamma'$  lattice misfit for the specific morphologies of the  $\gamma'$  precipitates. So according to literature [9] the samples were full solutioned at 1200°C for 2 hours in an atmospheric condition and then were cooled to 650°C under different cooling rates such as: air cooling (380°C/min), 15, 1, 0.2, 0.05 °C/min which are denoted with UAC, U15, U1, U0.2 and U0.05, respectively.

The heat treated specimens were mounted and polished using standard metallographic techniques for microstructural studies. Then they were electro-etched in an etchant containing 8%  $\text{H}_3\text{PO}_4$ , 28%  $\text{HNO}_3$ , 32%  $\text{H}_2\text{SO}_4$  and 32%  $\text{H}_2\text{O}$  for about 4 seconds under 2 volts DC current until developing a white halo at the surface of the specimens. This treatment dissolves the  $\gamma$  phase and leaves the  $\gamma'$  in relief [10]. The microstructures were studied using a scanning electron microscopy model *Cam Scan MV2300*, then were quantitatively analyzed using an image analyzer software, entitled *Clemex*.

For calculation the unconstrained lattice constant of the  $\gamma'$  precipitates and  $\gamma$ - $\gamma'$  misfit, the  $\gamma'$  precipitates of each specimen were electrolytically extracted and prepared as the powder samples for XRD analysis. The electrolytic extraction process was carried out using 0.18A/mm<sup>2</sup> current density in a  $\text{H}_2\text{O}$ -10 Vol.%  $\text{H}_3\text{PO}_4$  electrolyte. This technique completely dissolves the matrix phase  $\gamma$ , leaving a residue of all populations of the  $\gamma'$  and minor other phases, such as carbides and borides [8, 11]. The weight percent of the  $\gamma'$  in each sample was determined by the weight analysis of the primary samples and the extracted  $\gamma'$  powder. The XRD patterns were recorded using *CuK $\alpha$*  radiation in a *Brucker-Axs* machine equipped with a *D8-Advance* type model diffractometer. All of the X-ray scans were performed on the metallographically polished samples between 20 to 155

degrees with a step size of 0.005 degrees and step time of 1 second. Due to the oriented grains of the cast carrots, only a few peaks were appeared in the bulk samples. So the (111) peak of both, bulk and powder, samples was used for calculating the  $\gamma$ - $\gamma'$  misfit for all. In addition, the *Nelson-Riley* method [12] was applied for the precise calculation of the unconstrained lattice constant of the extracted  $\gamma'$  precipitates.

### 3. Results and discussion

Fig. 1 shows the microstructure of the bulk specimen heat treated at 1200°C for 2 hours followed by air cooling. The microstructure contains the squeezed together of the fine spherical  $\gamma'$  precipitates with very limited interparticle spaces.

Fig. 1. SEM micrograph of the bulk specimen, heat treated at 1200°C for 2 hours then air cooled.

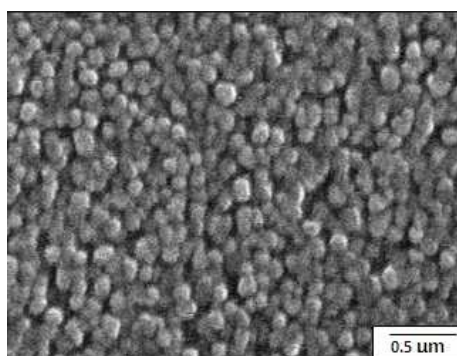


Fig. 2 shows how the morphology of the  $\gamma'$  precipitates is changed from cubic to flower-like then dendritic shape as the cooling rate is decreased.

Table 1 shows the average size, number density and weight percent of the  $\gamma'$  precipitates under different cooling rates. At higher cooling rates such as 15 °C/min or air cooling, due to higher undercooling, an explosive nucleation has been occurred which has led to the higher number density as well as smaller precipitates. However, at lower cooling rates, because of lower undercooling hence higher driving force for growth, this situation has been conversed. According to Table 1, it is also observed that as the cooling rate is decreased, the size and weight percent of the  $\gamma'$  precipitates has increased as well as their number density has decreased. It clearly implies that during the higher cooling rates the supersaturation of the matrix phase is not completely removed. So, as shown in Fig. 3 (a), it is expected that the matrix phase  $\gamma$  can lead to the larger lattice constants hence lower  $\gamma$ - $\gamma'$  lattice misfits according to Fig. 3 (b).

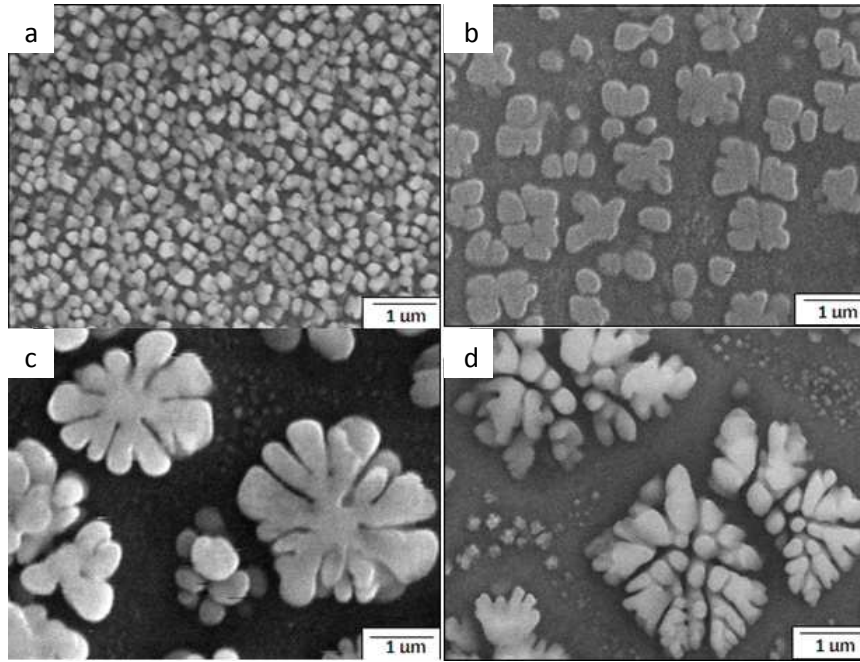


Fig. 2. SEM micrographs of the samples after 2 hours solutionizing at 1200°C and different cooling rates to ambient temperature: 15 (a), 1 (b), 0.2 (c) and 0.05 °C/min (d).

Table 1. The average size, number density and weight percent of the  $\gamma'$  precipitates under different cooling rates.

Cooling rate [°C/min]	AC	15	1	0.2	0.05
Number density [ $\mu\text{m}^{-2}$ ]	93	58	1.30	0.32	0.07
Average Size [ $\mu\text{m}$ ]	0.12	0.18	0.78	1.72	3.09
Weight percent	7.3	25.3	32.8	34	35.5

In fact, the morphological changes of the  $\gamma'$  precipitates in Fig. 2 are caused from variation of the  $\gamma$ - $\gamma'$  lattice misfit which can be attributed to variation of the chemistry of  $\gamma$  and  $\gamma'$  under different cooling rates. However, the practically stable values of the precise calculated lattice parameters for the extracted  $\gamma'$  in Fig. 3 (a) reveal their invariable chemical composition under different cooling rates. So it seems that the  $\gamma'$  precipitates reach to the equilibrium chemical composition during initial stages of the precipitation and their composition as well as lattice parameter is not changed during their subsequent growth or coarsening. In contrast, the considerable decreasing of the  $\gamma$  matrix phase lattice parameter by decreasing the cooling rate in Fig. 3 (a) is attributed to reduction of its solute concentration. Thus the increasing of the  $\gamma$ - $\gamma'$  unconstrained lattice misfit in Fig. 3 (b) is merely caused from decreasing of the lattice constant of the matrix phase  $\gamma$ . Furthermore, lower values of the constrained  $\gamma$ - $\gamma'$  lattice misfits in compared with unconstrained one in Fig. 3 (b) are resulted from the elastic strains in  $\gamma$ - $\gamma'$  interfaces which are observed for all of the cooling rates according to Fig. 4. So increasing of the lattice constant of the  $\gamma'$  precipitates in bulk sample (Fig. 3 (a)) through decreasing the cooling rate is not associated to the  $\gamma'$  chemical composition. It is attributed to decreasing of the compressive elastic strain on the  $\gamma'$  precipitates.

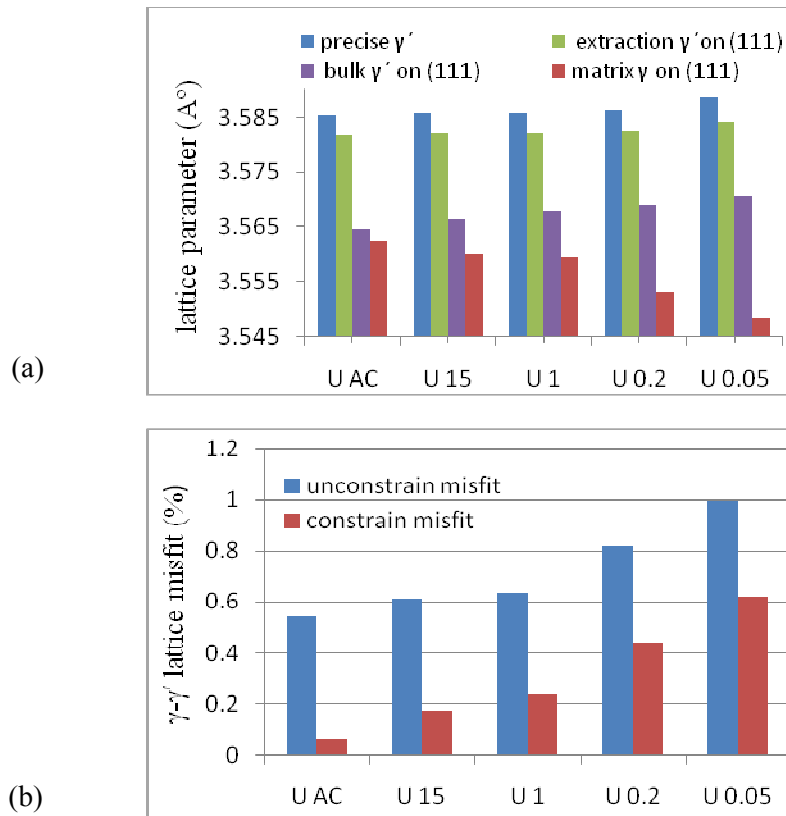


Fig. 3. Lattice constants of  $\gamma$  and  $\gamma'$  (a) and the constrained and unconstrained  $\gamma$ - $\gamma'$  lattice misfits on (111) planes (b) under different cooling rates.

Fig. 4 and the considerable differences between the constrained and unconstrained  $\gamma$ - $\gamma'$  lattice misfits in Fig. 3(b) both, indicate that the coherency between  $\gamma$  and  $\gamma'$  is not completely removed. Even for dendritic shape of the  $\gamma'$  precipitates corresponding to the slowest cooling rate, the interface between  $\gamma$  and coarsen  $\gamma'$  is semi-coherent rather than incoherent.

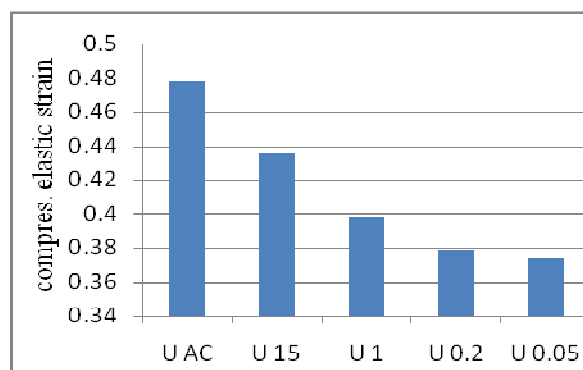


Fig. 4. Compressive elastic strain of the  $\gamma'$  precipitates under different cooling rates.

#### 4. Conclusion

The following results were obtained through studying the  $\gamma'$  precipitation in *Udimet 500* nickel-base superalloy during continues cooling under different cooling rates.

- 1) The  $\gamma'$  precipitates obtain an equilibrium chemical composition hence corresponding lattice constant in early stages of the precipitation. This lattice constant does not change during subsequent growth and coarsening. So the variation of the  $\gamma$ - $\gamma'$  lattice misfits in different cooling rates is caused from the compositional changes of the matrix phase and its corresponding lattice constant.
- 2) Through decreasing the cooling rate, not only the particle sizes and weight percent of the precipitates are increased but also the number density and the elastic strain of the  $\gamma'$  precipitates are decreased. Accordingly the corresponding morphology of the precipitates is changed from spherical to cuboidal then flower-like and finally dendritic shapes.
- 3) During continues slow cooling, the coherency between  $\gamma$  and  $\gamma'$  is not completely removed. For dendritic shape of the  $\gamma'$  attributed to the slowest cooling rate, 0.05 °C/min, the  $\gamma$ - $\gamma'$  interface is semi-coherent rather than incoherent.

#### References

- [1] T. Grosdidier, A. Hazotte, A. Simon: Mater. Sci. and Eng. A Vol. 256 (1-2) (1998), p. 183.
- [2] R.A. Ricks, A.J. Porter, R.C. Ecob: Acta Met. Vol. 31 (1) (1983), p. 43
- [3] S. Yeom, D. Yoon, M. Henry: Met. and Mat. Trans. A Vol. 24 (9) (1993), p. 1975
- [4] A.G. Khachaturyan, S.V. Semenovskaya, J.W. Morris Jr: Acta Met. Vol. 36 (6) (1988), p. 1563
- [5] Y.S. Yoo: *Scripta Mat.* Vol. 53 (1) (2005), p. 81.
- [6] M. Henry, Y. Yoo, D. Yoon, J. Choi: Met. and Mat. Trans. A Vol. 24 (8) (1993), p. 1733
- [7] D. Grose, G. Ansell: Met. and Mat. Trans. A Vol. 12 (9) (1981), p. 1631
- [8] R.J. Mitchell, M. Preuss, M.C. Hardy, S. Tin: Mat. Sci. and Eng. Vol. A 423 (1-2) (2006), p. 282
- [9] S.A. Sajjadi, H.R. Elahifar, H. Farhangi: J. of Alloys and Comp. Vol. 455 (1-2) (2008), p. 215
- [10] S. Behrouzghaemi, R.J. Mitchell: Mat. Sci. and Eng. A Vol. 498 (1-2) (2008), p. 266
- [11] S. Soleimani, A. Abdollah-Zadeh, A. Samadi, H. Assadi: J. of Optoelectronics and Advanced Materials Vol. 9 (6) (2007), p. 1789
- [12] B.D. Cullity: *Elements of X-ray Diffraction* (Addison-Wesley Pub. Co., USA 1977).